A reduced order numerical model for high-pressure hydrogen leak self-ignition

Marc Le Boursicaud, Song Zhao, Jean-Louis Consalvi, Pierre Boivin

A reduced order numerical model for high-pressure hydrogen leak self-ignition

Marc Le Boursicaud[a,*], Song Zhao[a], Jean-Louis Consalvi[b], Pierre Boivin[a]

[a] *Aix Marseille Univ, CNRS, Centrale Med, M2P2, Marseille, France*
[b] *Aix Marseille Univ, CNRS, IUSTI, Marseille, France*

Abstract

The numerical study of ignition risk in the event of high-pressure hydrogen leakage presents numerous challenges. The first is to properly simulate the complex multi-dimensional flow (hemispherical expanding shock and contact discontinuity). The second is to properly resolve the diffusion/reaction interface, which has a very small length scale compared to the jet radius. We propose a low-order numerical model for such flows by first decoupling the flow and the diffusion/reaction interface into one cold flow and one reaction interface problem. The flow can be further simplified by assuming a "pseudo" 1D model with corrective source terms to account for axisymmetric (for a 2D test case) or spherical effects. Meanwhile, the diffusion interface is solved with a different space variable to optimize the mesh while using the results of flow simulation. The interface problem is further simplified by using the passive scalar approach recently developed for hydrogen ignition prediction (Le Boursicaud et al., Combust. Flame 256 (2023) 112938). Validation of the flow and interface solver is achieved through simple test cases, and the full configuration results are compared to the state-of-the-art model of the literature (Maxwell and Radulescu, Combust. Flame 158 (2011) 1946-1959).

Novelty and Significance Statement: In order to study the risk of shock-induced self-ignition of high-pressure hydrogen leakage, a new approach is developed by considering the flow to be pseudo-1D. This pseudo-1D model uses a specific source term in the governing equations, allowing for a drastic computational cost reduction compared to 2D-axisymmetrical or 3D simulations while being more general than partial models found in the literature. This source term is found to be independent of the hydrogen storage pressure

[*] Corresponding author.
Email address: marc.leboursicaud@gmail.com (Marc Le Boursicaud)

and leakage radius. Moreover, a recently developed passive scalar approach was introduced for the first time to predict ignition within a dynamic diffusion layer.

Authors Contributions Statement:
-M.LB. : Designed research, Software, Formal analysis, Writing - original draft
-S.Z. : Supervision, Methodology, Writing - review & editing
-JL.C. : Supervision, Methodology, Writing - review & editing
-P.B. : Supervision, Methodology, Funding acquisition, Writing - review & editing

Keywords: Shock-induced ignition, Reduced-order model, Leakage, Hydrogen safety

---

1. Introduction

1.1. Problem description

The increasing use of hydrogen as a carbon-free fuel in the transport and industrial sectors raises some safety issues. Although the canonical hydrogen ignition cases are now well understood [1] (explosion limits, minimum ignition energy, diffusion layer ignition), there is still a lack of understanding and development of adequate tools for more complex configurations. We are especially interested in hydrogen leakage from a high-pressure tank that may lead to shock-induced ignition.

We consider a high-pressure tank filled with hydrogen, abruptly leaking into ambient air through a hole of a given radius as illustrated in Fig. 1. This initially leads to a classical shock tube solution, with hydrogen cooled by the rarefaction wave separated from the shock-heated air by the contact discontinuity. It is rapidly followed by the formation of a jet and its expansion. This expansion directly implies a decay of the pressure around the contact, translated by a general cooling and so a reduction of reactivity in the diffusion layer. The ignition may occur if the expansion rate of the jet is not strong enough to quench the ignition process. The temperature, pressure, hydrogen mass fraction, and density gradient field of a non-reactive two-dimensional simulation performed with the compressible code ProLB [2, 3] (based on lattice Boltzmann methods) are shown in Fig. 2. We can observe the most important features (from right to left) the leading shock wave, the contact discontinuity, and the formation of the Mach shock. Close to the contact, the center line holds the highest temperature, making it the most likely place to ignite due to the presence of both hydrogen and air.

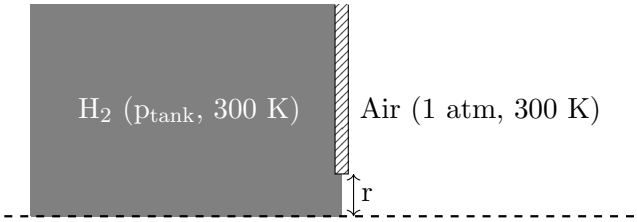

Figure 1: Sketch of the configuration, dashed line: axis of symmetry.

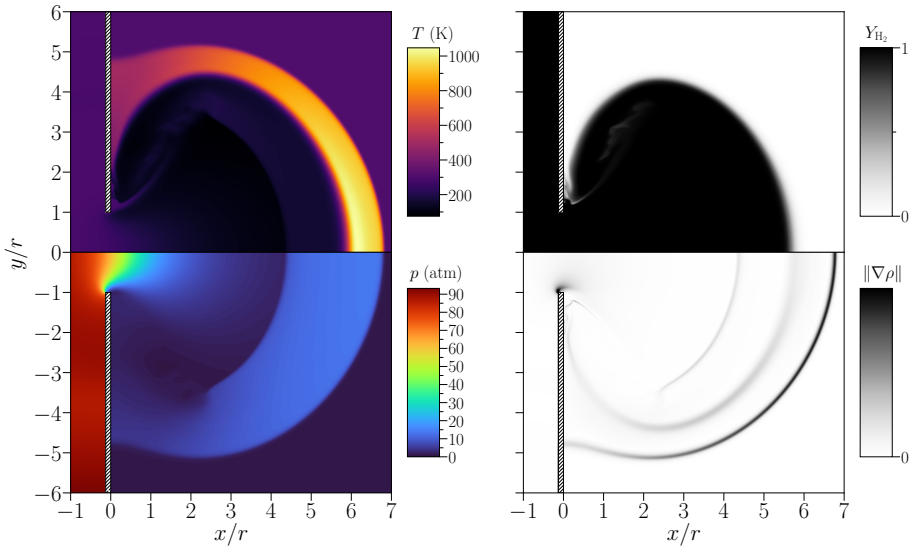

Figure 2: Temperature (top left), pressure (bottom left), hydrogen mass fraction (top right) and density gradient (bottom right) fields obtained with ProLB [2] for a hydrogen tank pressure of p_{tank}=100 atm and a leakage radius of r=2 mm at a time t=10 µs.

1.2. Previous studies

The ignition of pressurized hydrogen release into the air has first been postulated and observed by Wolański and Wójcicki [4]. Similar observations were made in Refs. [5–8] and highlighted two key parameters: the tank pressure, p_{tank}, and the leak hole radius, r. It has also been shown in Ref. [9] that hydrogen is more prone to this kind of ignition due to its low Lewis number, compared to hydrocarbon fuels, as the fuel needs to rapidly diffuse into the shock-heated air.

Maxwell and Radulescu proposed a simplified model to obtain numerically the limit condition for ignition [10]. It consists of separating the problem into two sub-problems: the flow in one part and the diffusion layer

in another one. On top of that, DNS simulations were recently performed in Ref. [11] to study the effect of an obstacle placed in front of the leakage, representative of confined space configurations. They show that high-pressure leakage in confined space is more prone to ignition than in open space due to the reflected shock wave heating up the diffusion layer as it passes through it. However, DNS of this kind of configuration is heavily dependent on their grid size. Figure 3 illustrates the effect of the space resolution on the temperature (left panel). The reactivity - or inverse ignition characteristic chemical time - as introduced by Boivin et al. [1, 12] is also plotted (right panel). Due to the Arrhenius exponential dependence on temperature, a small temperature difference yields large reactivity discrepancies on the center line of the jet. The finest spatial resolution is needed to recover the correct temperature peak, but also to correctly resolve the diffusion layer and especially the profiles of the radicals created within this thin layer. The diffusion layer is the smallest length scale with a thickness of 1 to 100 µm whereas the distance traveled by the leading shock is the largest one, ranging from 1 to 100 cm at the ignition time. The objective of this study is then to develop of a reduced-order model rather than performing DNS which will require at least adaptive mesh refinement with the cost associated.

Therefore, we propose to validate a new method, inspired by the one proposed by Maxwell and Radulescu [10] but more general, in order to first recover the ignition limit for open space configuration and to apply it to more complex configurations such as confined space in future works.

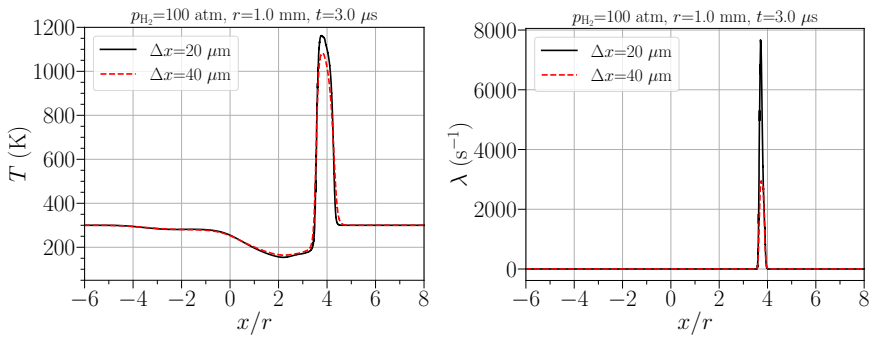

Figure 3: Temperature and reactivity (branching rate) profiles on the center line for two different resolutions.

2. Previous modeling methodology

The model proposed by Maxwell and Radulescu [10] is based on scale separation. As mentioned previously there is almost three orders of magnitude differences between the diffusion interface thickness and the distance traveled by the leading shock for this problem. The scale separation is achieved by using a Lagrangian approach following the contact discontinuity for the diffusion layer, solving only the mass fractions and the temperature on a one-dimensional domain. The pressure and velocity in the diffusion layer are assumed to be uniform, as they remain continuous along a contact discontinuity, and the diffusion layer is thin enough to neglect their gradients.

2.1. The diffusion layer

In order to properly study the diffusion layer, a change of variable is often made to keep a compact domain accounting for the physical thickening of the diffusion layer over time. Maxwell and Radulescu [10] used a mass-weighted variable m defined as:

$$m = \int_0^x \rho(x,t)dx, \tag{1}$$

leading to:

$$\frac{\partial}{\partial x} = \rho\frac{\partial}{\partial m}. \tag{2}$$

Using this new variable, the set of equations that are considered for the diffusion layer are:

$$\rho\frac{\partial Y_k}{\partial t} = \omega_k - \rho\frac{\partial \rho Y_k V_k}{\partial m} \tag{3}$$

$$\rho c_p\frac{\partial T}{\partial t} = \frac{Dp}{Dt} - \sum_k h_k\omega_k + \rho\frac{\partial}{\partial m}\left(\rho\kappa\frac{\partial T}{\partial m}\right) - \sum_k \rho^2 Y_k V_k c_{p,k}\frac{\partial T}{\partial m} \tag{4}$$

with:

$$Y_k V_k = -D_k\frac{W_k}{W}\rho\frac{\partial X_k}{\partial m} + Y_k V_c \tag{5}$$

$$V_c = \sum_k D_k\frac{W_k}{W}\rho\frac{\partial X_k}{\partial m} \tag{6}$$

D_k and κ are the mixture average diffusion coefficient and thermal conductivity given by Cantera [13]. It should be noted that the perfect gas equation

of state is used, and non-ideal thermodynamic properties (which vary with temperature) based on the NASA 7 polynomials are used unless otherwise stated. In addition, the left and right boundary conditions (denoted by index L and R respectively) are:

$$Y_{k,L} = \begin{cases} 1.0, & \text{if } k = \mathrm{H_2} \\ 0.0, & \text{otherwise} \end{cases} \tag{7}$$

$$Y_{k,R} = \begin{cases} 0.233, & \text{if } k = \mathrm{O_2} \\ 0.767, & \text{if } k = \mathrm{N_2} \\ 0.0, & \text{otherwise} \end{cases} \tag{8}$$

$$\frac{dT_L}{dt} = \frac{1}{\rho_L c_{p,L}} \frac{Dp}{Dt} \tag{9}$$

$$\frac{dT_R}{dt} = \frac{1}{\rho_R c_{p,R}} \frac{Dp}{Dt}. \tag{10}$$

To solve the evolution of the entire diffusion layer, the initial temperatures on both sides of the initial contact discontinuity are required (obtained with a classical Riemann solver [14]) as well as the evolution of the pressure within the diffusion layer. The way to determine the pressure evolution will be discussed in the next Section in the framework of the model proposed by Maxwell and Radulescu [10] and in Section 3 for the specific model proposed in the present study.

2.2. Simple pressure decay model

Radulescu and Law [15] previously obtained an analytical model for the pressure evolution at the contact through the study of transient supersonic jets. It was however replaced by a fitted power-law in the Maxwell and Radulescu model [10], due to its simplicity and better precision. This fit is only valid for a three-dimensional configuration of a hydrogen tank discharging into ambient air through a circular hole:

$$p_{\mathrm{contact}}/p_{\mathrm{air},0} = 12.2\tau^{-0.68}. \tag{11}$$

where the non-dimensional time, τ, is given by:

$$\tau = t \left(\frac{\rho_{\mathrm{air},0}}{\rho_{\mathrm{H_2},0}} \left(\frac{2}{\gamma_{\mathrm{H_2},0}+1} \right)^{-1/(\gamma_{\mathrm{H_2},0}+1)} \right)^{1/2} \frac{c_{\mathrm{H_2},0}}{1.2r} \left(\frac{2}{\gamma_{\mathrm{H_2},0}+1} \right)^{1/2}, \tag{12}$$

with c and γ standing for the speed of sound and the heat capacity ratio respectively, while subscript "o" stands for the initial tank or ambient air conditions. From Eqs. (11) and (12) we obtained the source term needed in Eq. (4):

$$\frac{Dp}{Dt} = -8.3 p_{\mathrm{air},0} \frac{\partial \tau}{\partial t} \tau^{-1.68}. \tag{13}$$

Using all the frameworks described earlier, the solution of a typical diffusion layer is shown in Fig. 4. The figure highlights the cooling effect due to the flow expansion on the temperature profiles (right panel), as well as the ignition site, clearly situated on the air side due to the higher temperature and the low Lewis number of the hydrogen molecule. Figure 4 also shows the efficiency of the coordinate m to keep a compact mesh, as the hydrogen mass fraction (left panel) barely changed over time in this framework.

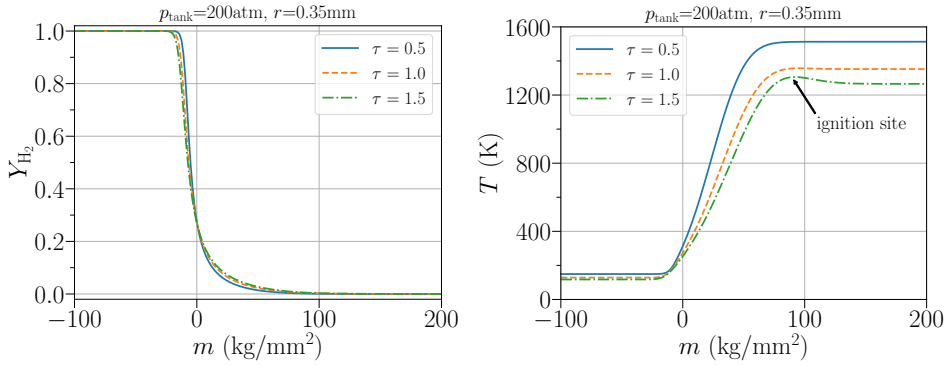

Figure 4: Hydrogen mass fraction and temperature profile in the diffusion layer at three different times for an initial hydrogen storage pressure of p_{tank}=200 atm and a leakage radius of r=0.35 mm.

3. Pseudo 1D flow for high pressure leakage

In this section, we propose an alternative to the model presented in Section 2.2 to obtain the pressure evolution. A source term $\mathcal{S}$ is used to model the transition of the waves from planar to spherical (or cylindrical in 2D). This allows pseudo-1D modeling of the flow along the center line (where the conditions are the most favorable for ignition), the source term accounting for the flow expansion. The generalized Euler equations (for two species) are given by:

$$\frac{\partial \rho}{\partial t} + \frac{\partial \rho u}{\partial x} = -\mathcal{S}(x,t)\rho u \tag{14}$$

$$\frac{\partial \rho u}{\partial t} + \frac{\partial \rho u u + p}{\partial x} = -\mathcal{S}(x,t)\rho u u \tag{15}$$

$$\frac{\partial \rho E}{\partial t} + \frac{\partial \rho u E + p u}{\partial x} = -\mathcal{S}(x,t)\left(\rho u E + p u\right) \tag{16}$$

$$\frac{\partial \rho Y_{\mathrm{H_2}}}{\partial t} + \frac{\partial \rho u Y_{\mathrm{H_2}}}{\partial x} = -\mathcal{S}(x,t)\rho u Y_{\mathrm{H_2}} \tag{17}$$

where E denotes the total energy per unit of mass. In the limit of 2D cylindrical or 3D spherical symmetry flows, the exact source term is given by:

$$\mathcal{S}_{\mathrm{sym}} = \frac{\alpha}{x}. \tag{18}$$

The parameter α is related to the dimension of the problem: α=0 for one-dimensional flows, α=1 for cylindrical, and α=2 for spherical ones. This allows to recover the classical Euler equations for cylindrical and spherical symmetry as written in Ref. [14] (section 1.6.4). In our case, the shape of $\mathcal{S}$ will be different, as it is introduced to describe the flow transition from planar to spherical (or cylindrical in 2D) once the expansion starts on the centerline

3.1. Onset time of the pressure decay

The first key point for our pseudo-1D model is to predict when the expansion starts on the center line, as the waves are considered to remain perfectly planar before that. Radulescu and Law [15] showed that expansion waves, generated from the leakage edge as the shock passes through it, are responsible for the start of the flow expansion. Those waves propagate at the local sound speed with respect to the flow. Therefore the first wave to reach the center line is traveling purely normal to the flow. As the leading shock wave and the contact discontinuity are infinitely close initially, this first expansion wave reaching the center line is following the contact, both of them being advected by the flow. Hence, two candidates for the fastest wave appear, each one traveling on each side of the contact. Depending on the initial tank pressure, the initial shock tube solution leads to the left side (with hydrogen) or the right side (with air) having a faster speed of sound. Figure 5 shows a simplified sketch for the two possible cases, with a faster speed of sound on the hydrogen side for the left panel and on the air side

for the right panel. The leading shock wave and contact discontinuity are shown, as well as the simplified expansion waves generated on both sides.

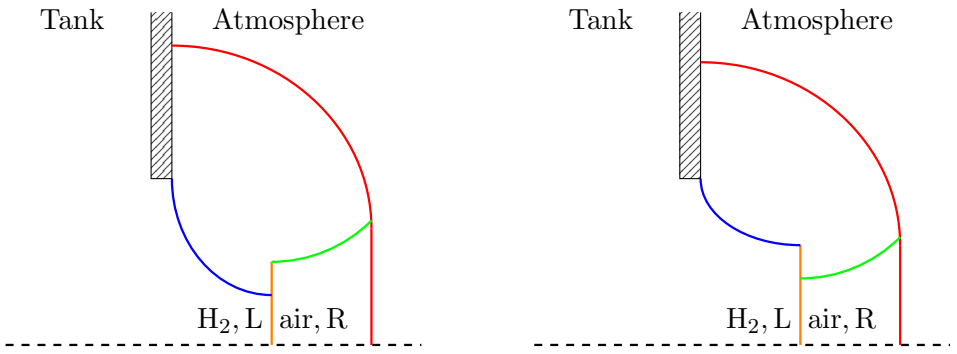

Figure 5: Sketch of the early waves generated. The red and orange curves correspond respectively to the leading shock and contact discontinuity. The blue and green curves represent the expansion wave generated on either side of the contact. The two sketches correspond to two scenarios with different pressures of the hydrogen tank.

Using the initial shock tube solution with the state "L" and "R" respectively on the left and right side of the contact (corresponding to the post-rarefaction for the hydrogen and post-shock for the air and are therefore different from the initial tank and ambient states), it is easy to determine the traveling time of the first wave reaching the center line. Therefore the time t_E at which the source term should be activated is given by:

$$t_E = \min\left(r/c_{\mathrm{H_2,L}}, r/c_{\mathrm{air,R}}\right). \tag{19}$$

This analytical prediction is compared in Fig. 6, on the one hand, with the dimensionless time at which the pressure starts to decay for the model from Ref. [10] and, on the other hand, with 2D Euler simulations performed with ECOGEN [16]. ECOGEN is a multiphase compressible solver, with an axisymmetric formulation that will be used later. It shows that the time at which the pressure starts to decay is well predicted by the present analytical expression, Eq. (19). It can also be observed that it provides a slightly better agreement than the power-law model proposed by Maxwell and Radulescu [10].

3.2. Profile of the source term coefficient

We now need to determine the spatial shape of $\mathcal{S}$ to make the flow transition from planar to spherical (or cylindrical in 2D). We know that far from the leakage it should fall back to α/x, however, its shape around the

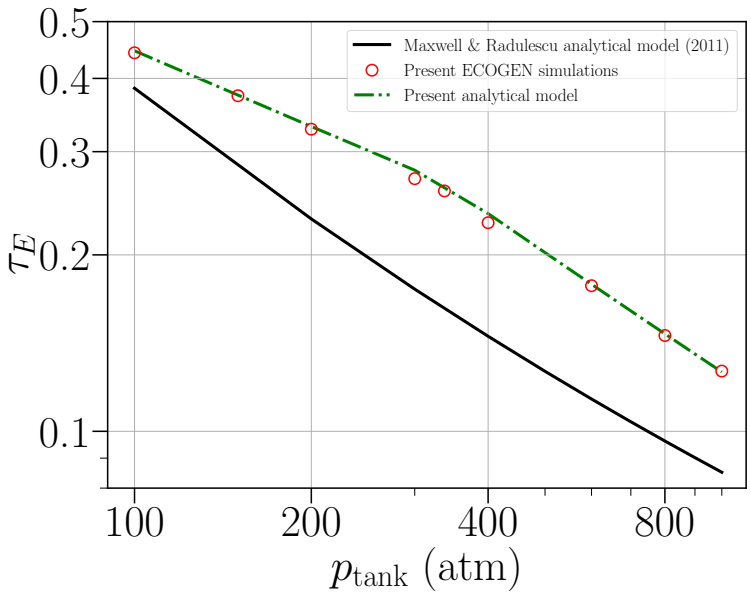

Figure 6: Comparison of the time at which the expansion waves created by the hole edge reaches the center-line, for 2D ECOGEN [16] simulations, Maxwell and Radulescu model and our analytical model given by Eq. (19).

leak is unknown. In order to account for 2D or 3D effects, the source term is introduced as a correction to recover the divergence operator. Apply to $\rho\mathbf{u}$, it gives :

$$div(\rho\mathbf{u})_{\text{pseudo}-1\text{D}} = \frac{\partial \rho u_x}{\partial x} + red\rho u_x \mathcal{S} = \frac{\partial \rho u_x}{\partial x} + \alpha \frac{\partial \rho u_y}{\partial y} = div(\rho\mathbf{u}). \quad (20)$$

Therefore, the source term is equal to :

$$\mathcal{S} = \alpha \frac{\partial \rho u_y}{\partial y} / \rho u_x. \quad (21)$$

The source term $\mathcal{S}$ will be obtained by fitting Eq. (21) from the 2D simulations performed with ECOGEN [16]. The fitted expression is:

$$\mathcal{S}(x,t) = \begin{cases} 0, & \text{if } t < t_E \\ \frac{\alpha}{r} \frac{6\chi^3 - 9\chi^2 + 38\chi - 18}{6\chi^4 - 12\chi^3 + 39\chi^2 - 17\chi + 33}, & \text{otherwise} \end{cases}, \quad (22)$$

with $\chi = x/r$ the dimensionless coordinate where negative values correspond to the tank interior. Figure 7 shows $\mathcal{S} \times r/\alpha$ as a function of $\chi = x/r$.

This figure confirms that the self-similar profile given in Eq. (22) reproduced very well the shape of the source term obtained with ECOGEN whatever the pressure, the leakage size, and the dimension of the problem. Although the model was fitted using the 2D simulations obtained with ECOGEN, explaining the small difference observed for the 3D case in Fig. 7, it was found to have no impact on the final ignition limits. It should also be pointed out that, as expected, Eq. (22) tends toward α/x far from the leakage.

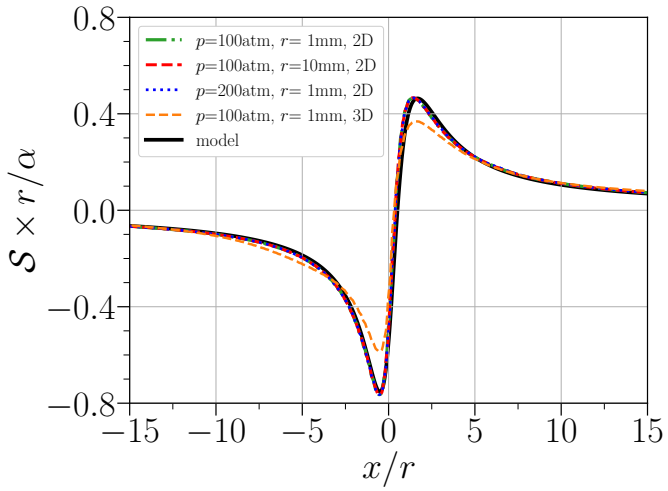

Figure 7: Comparison of the different dimensionless source term coefficient $\mathcal{S}$ profiles, obtained as post-treatment of ECOGEN [16] 2D and 3D (2D axisymmetrical) simulations, as well as the present model.

3.3. Flow prediction with the source term

The pseudo-1D flow solver uses a MUSCL-Hancock scheme (where the source term is considered for the prediction step) along the HLLC solver. The multidimensional simulations of reference were performed with ECOGEN [16]. For all simulations, both ECOGEN and the present pseudo-1D code used the MUSCL scheme with HLLC to achieve second-order accuracy with the van Albada slope limiter. For this comparison only, the pseudo-1D code used constant thermodynamic properties, as used by ECOGEN (γ_{H_2}=γ_{air}=1.4).

The resulting comparisons of the velocity and pressure profiles along the center line are shown in Fig. 8 for the same conditions as in Fig. 2.

For a three-dimensional leakage, the resulting profiles are compared in

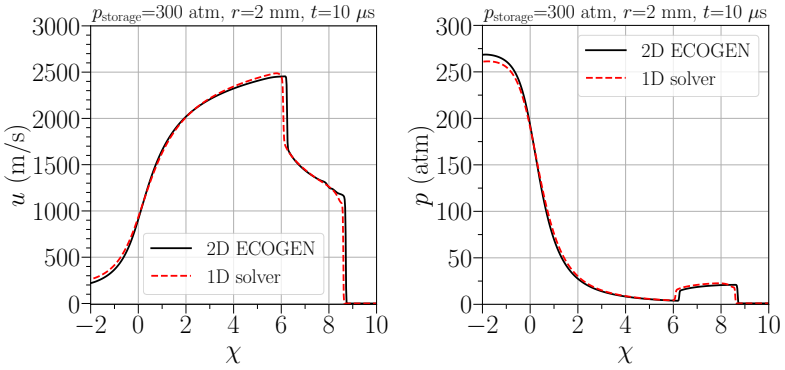

Figure 8: Comparison of the velocity and pressure profiles in the center line for a 2D simulation with ECOGEN [16] and with the pseudo-1D solver using the source term Eq. (22).

Fig. 9, this time, the simulation of reference uses a 2D axisymmetrical formulation.

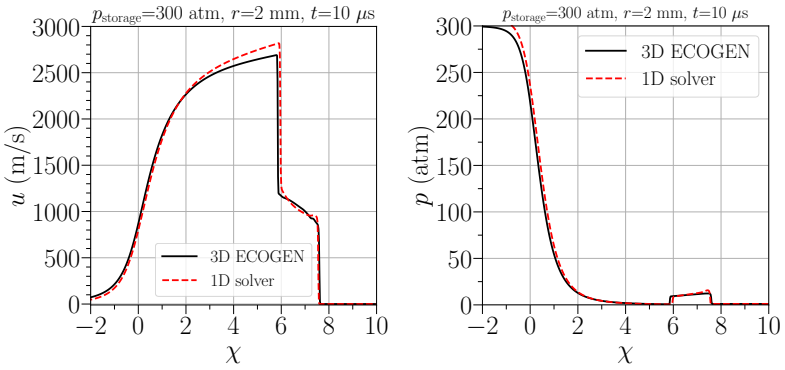

Figure 9: Comparison of the velocity and pressure profiles in the center line for a 3D (2D axisymmetrical) simulation with ECOGEN [16] and with the pseudo-1D solver using the source term Eq. (22).

Despite minor differences, our model is capable of predicting the flow features and their dynamics, including the prediction of the Mach disk and the leading shock position, visible in Figs. 8 and 9 (respectively the left and right discontinuity). Therefore, it is an interesting option to study this type of configuration, especially as it is more general than the approach of Maxwell & Radulescu [10], as it can be applied to various kinds of leakage (2D/3D, tank/pipe) and various other gases, including methane and propane, and initial pressurized gas and air temperatures, as shown in Appendix D.

4. Validation of the passive scalar approach for the diffusion interface ignition

To further simplify the problem, we propose to use the passive scalar approach recently developed in Refs. [3, 17]. The principle of this approach is to only solve the transport equation for the main species (H_2, O_2, N_2) without considering reactions or heat release, therefore ignoring the 5 radicals (H, O, OH, HO_2 and H_2O_2) and the only combustion product H_2O. Instead, a self-reactive scalar, noted η, is used to model the ignition process. This scalar is said to be passive as it does not affect the flow which only considers the main species, and it follows a classical reaction-diffusion type transport equation. After simplification of Eqs. (3) and (4) for only two species (O_2 and N_2 are now considered with the equivalent specie air, more details in Appendix A), the set of equations solved (using the same boundary conditions as in section 2.1) when considering the scalar is:

$$\rho\frac{\partial Y_{\mathrm{H_2}}}{\partial t} = \rho\frac{\partial}{\partial m}\left(\rho^2 D_{\mathrm{H_2}}\frac{W_{\mathrm{H_2}}}{W}\frac{\partial X_{\mathrm{H_2}}}{\partial m}\right) \tag{23}$$

$$\rho c_p\frac{\partial T}{\partial t} = \frac{Dp}{Dt} + \rho\frac{\partial}{\partial m}\left(\rho\kappa\frac{\partial T}{\partial m}\right) + \frac{\rho^3}{W}\frac{\partial T}{\partial m}\sum_k D_k W_k c_{p,k}\frac{\partial X_k}{\partial m} \tag{24}$$

$$\rho\frac{\partial Y_\eta}{\partial t} = \omega_\eta + \rho\frac{\partial}{\partial m}\left(\rho^2 D_\eta\frac{W_\eta}{W}\frac{\partial X_\eta}{\partial m}\right) \tag{25}$$

with:

$$\omega_\eta = W_\eta\left(\omega_5 + \lambda C_\eta + \frac{1}{2}qC_\eta^3\right). \tag{26}$$

This scalar formulation is based on an eigenmode analysis of radical production, enabling the analytical recovery of the dominant mode (i.e., λ) associated with chain-branching [18]. The reactions considered in this eigenmode analysis are those of an 8-step skeletal mechanism previously employed in ignition studies [1, 18, 19]. This mechanism includes initiation, branching, and termination reactions necessary to accurately model autoignition. It should be noted that no noticeable differences can be observed, when using the skeletal mechanism or the detailed mechanism used in [10] in the final ignition limit, as highlighted in Appendix B, motivating the use of the skeletal mechanism for its simplicity. The scalar approach was initially developed (using only the ω_5 and λ terms) for 3D simulations to predict the lift-off of a hydrogen jet flame at atmospheric pressure [3]. To account

for the specific characteristics of hydrogen chemistry at high pressure (e.g. thermal runaway and non-linearity) the formulation was recently enhanced [17]. Notably, the cubic term, $\frac{1}{2}qC_\eta^3$, was introduced as a correction to account for the increase in reaction rates with rising temperature, thereby compensating for the absence of heat release in the model.

Figure 10 shows the difference in hydrogen mass fraction and temperature profiles in the diffusion layer when solving for the 9 reactive species or only 2 non-reactive species (H_2, air) with the scalar. The only small differences in the hydrogen mass fraction profile mainly results from the absence of differential diffusion between O_2 and N_2 for the 2 species model as they are regrouped into the equivalent air specie. A larger difference is observed for the temperature profile. It directly comes from the heat release considered for the 9 species model but not when using the scalar approach. This highlights the location where the ignition takes place. Figure 11 shows the temporal evolution of the maximum temperature and OH mass fraction within the diffusion layer. The 9 species model displays a slower temperature decay at the end as the heat released by the reactions is no longer negligible compared to the expansion cooling effect. Whilst neglecting the heat release, resulting in a lower maximal temperature in the domain, the scalar approach properly recovers the ignition process (thanks to the recent development made as explained earlier) as highlighted by the OH mass fraction evolution. As in Ref. [10], ignition is considered to occur when the OH mass fraction reaches 10^{-3}.

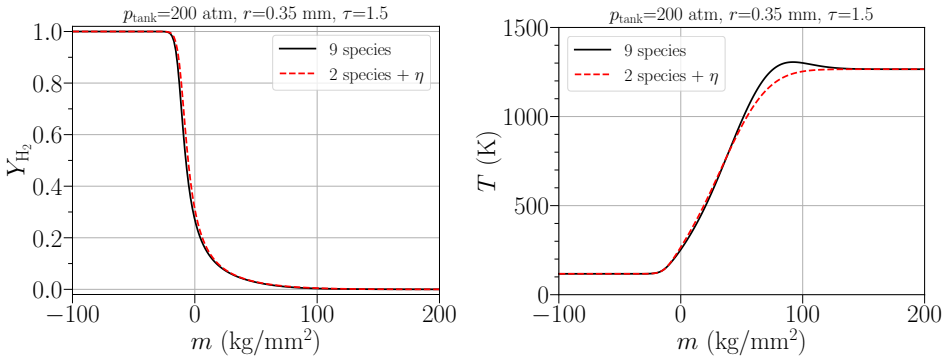

Figure 10: Hydrogen mass fraction and temperature profiles in the diffusion layer at a time τ=1.5 (t=1.56 µs) for an initial hydrogen storage pressure of p_{tank}=200 atm and a leakage radius of r=0.35 mm. The black curve is obtained when considering the 9 reactive species while the red curve is obtained for 2 non-reactive species in addition to the self-reacting passive scalar.

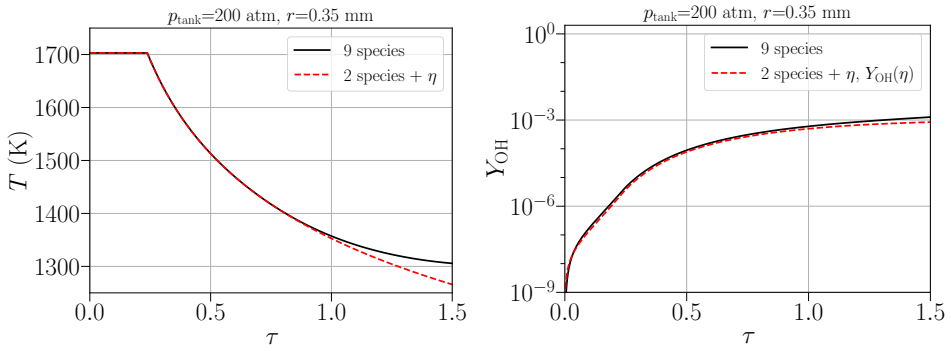

Figure 11: Evolution over time of the maximal temperature and OH mass fraction in the diffusion layer for an initial hydrogen storage pressure of p_{tank}=200 atm and a leakage radius of r=0.35 mm. The black curve is obtained when considering the 9 reactive species while the red curve is obtained for 2 non-reactive species in addition to the self-reacting passive scalar.

For the scalar model, the OH radical is not directly solved. It is obtained in a post-treatment using the scalar mass fraction and the local eigenvector associated with branching mode, which represents the radicals molar fractions in the radical-pool. This eigenvector is also used to obtain the diffusion coefficient D_η, defined as the weighted average of the diffusion coefficient of the different radicals present for the local conditions. More details can be found in [17].

It is also important to mention the impressive gain obtained by using only 2 species together with the scalar, which is about 50 times faster than solving the diffusion layer for the 9 reactive species.

5. Final results

5.1. Comparison of the methodologies

Finally, the ignition limits can be obtained using the model presented earlier, for a given hydrogen storage pressure, the critical leakage radius is obtained with the bisection method. For a tested value of r, the modeled flow is simulated with the 1D code and the pressure evolution at the contact is saved. Then the diffusion layer is simulated using this pressure evolution (Eqs. (23)-(25)). If the OH mass fraction in the diffusion layer reaches somewhere the threshold value of 10^{-3}, we consider it as an ignition event, otherwise, it's a failed ignition. We know that the critical radius is smaller than a tested radius if it leads to ignition and larger otherwise. Therefore,

the value of the critical radius is refined using the bisection method until a relative difference of less than 1% is reached.

Figure 12 shows the ignition limit obtained with the present methodology described above and the one with the original methodology proposed by Maxwell & Radulescu [10]. The present model is in excellent accordance with their model, experimental tests [7] and other multi-dimensional studies [11, 20, 21].

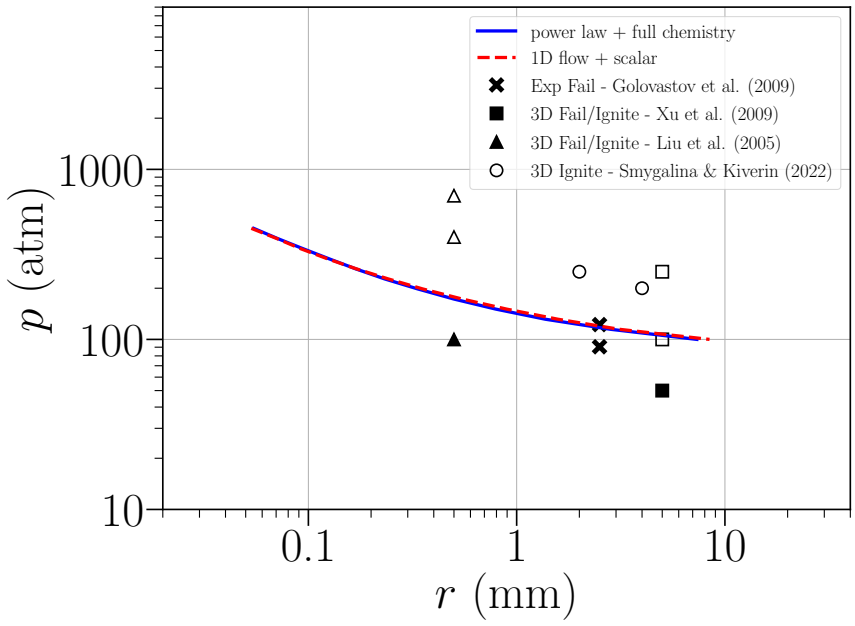

Figure 12: Comparison of the ignition limits obtained for the original and present approach.

5.2. Effect of the geometry

The present methodology is also more general as it allows to study other geometries. For example, the ignition limit for a planar tank leakage are obtained by using α=1 in Eq. (22) instead of α=2 for a 3D leakage. We can also study leakage from a high-pressure pipe instead of a tank, as done in [7, 11]. This geometry is illustrated in Fig. 13 and uses the same key parameters (p, r). The flow for this pipe configuration is obtained by using a different shape for the source term coefficient, more can be found in Appendix C.

The ignition limits of the tank and pipe configurations for both 2D and 3D cases are displayed in Fig. 14. It shows that the geometry has no impact

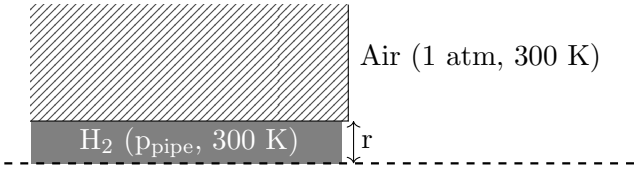

Figure 13: Sketch of the pipe configuration, dashed line: axis of symmetry.

on large leakage sizes. However, planar leakage better promotes ignition than more realistic 3D ones (due to the jet expanding in only one extra direction instead of two, leading to a slower cooling rate). The same is observed for the tank geometry over the pipe one, as it can provide a higher leakage flow rate and so a slower expansion, allowing the ignition to occur before the quenching. Those results are in agreement with the recent study [11].

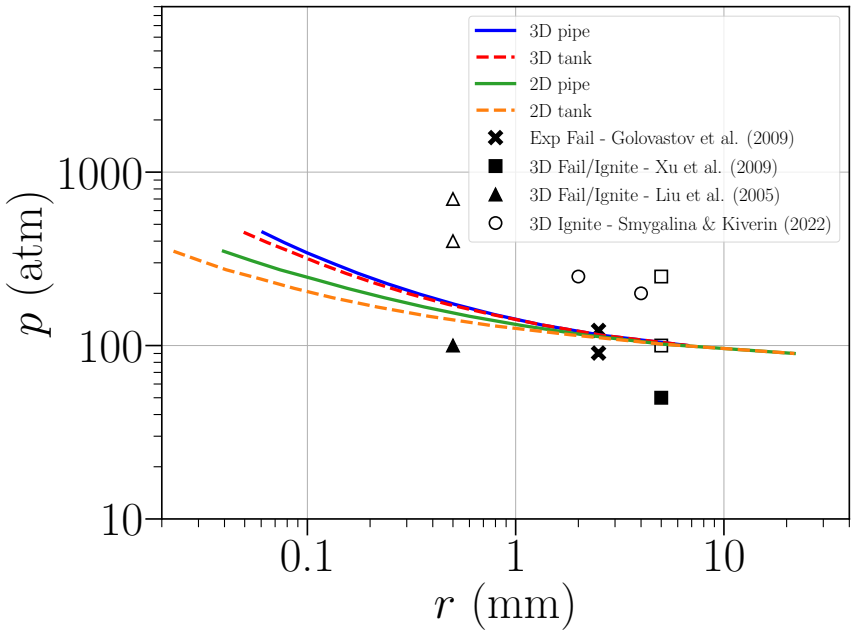

Figure 14: Comparison of the ignition limits obtained for different geometries

It is also important to mention that the time needed to solve the pseudo-1D flow is less important than the time saved when using the scalar approach for the diffusion layer instead of solving detailed chemistry for the 9 species. Overall the present method is faster than the original one thanks to that.

For given conditions (p, r) it takes less than a minute for the algorithm to predict whether the flow is prone to ignition or not.

6. Conclusions

We proposed a new approach to numerically study high-pressure hydrogen tank leakage into ambient air, leading to excellent agreement with the previous studies of the literature. This method is based on modelling and simulation of the flow as a pseudo-one-dimensional flow with a specific source term to account for the multi-dimensional effects such as the natural expansion of the jet created.

To the authors' knowledge, this simple model, blending 1D and 2D/3D using planar/cylindrical/spherical coordinates in a single formulation is the first of its type and was found to be valid not only for a large range of tank/pipe pressures, but also for various other pressurized gases and initial temperatures, as highlighted in Appendix D.

This flow model allows to recover the pressure evolution at the site most likely to ignite, the interface between the cold hydrogen and the hot air on the center line. This pressure evolution is required to account for the natural cooling of the flow and to properly predict the ignition process recover with a dedicated diffusion layer solver. On top of obtaining excellent results with this model compared to the original one, our methodology is faster thanks to using a passive scalar approach that replaces the radicals and reactions while recovering the correct ignition history. Overall, this paper validates this methodology, a required first step before considering more complex configurations and geometries where reflected waves must be considered for hydrogen safety.

7. Acknowledgments

Part of this research was supported by the French project BALBUZARD funded by DGAC and supported by Next generation EU in the frame of "Plan national de Relance et de Résilience français (PNRR)" ; and by the ANR, Airbus, Fives-Pillard and SafranTech through the Industrial Chair Program LIBERTY ANR-23-CHIN-0005.

References

[1] P. Boivin, M. Le Boursicaud, A. Millan-Merino, S. Taileb, J. Melguizo-Gavilanes, F. A. Williams, Hydrogen ignition and safety, in: Hydrogen for future thermal engines, Springer, 2022.

[2] M. Tayyab, S. Zhao, Y. Feng, P. Boivin, Hybrid regularized lattice-boltzmann modelling of premixed and non-premixed combustion processes, Combust. Flame 211 (2020) 173–184.

[3] S. Taileb, A. Millán-Merino, S. Zhao, P. Boivin, Lattice-boltzmann modeling of lifted hydrogen jet flames: a new model for hazardous ignition prediction, Combust. Flame 245 (2022) 112317.

[4] P. Wolanski, Investigation into the mechanism of the diffusion ignition of a combustible gas flowing into an oxidizing atmosphere, in: Symp. (Int.) Combust. 14, 1973.

[5] F. L. Dryer, M. Chaos, Z. Zhao, J. N. Stein, J. Y. Alpert, C. J. Homer, Spontaneous ignition of pressurized releases of hydrogen and natural gas into air, Combust. Sci. Technol. 179 (2007) 663–694.

[6] T. Mogi, Y. Wada, Y. Ogata, A. K. Hayashi, Self-ignition and flame propagation of high-pressure hydrogen jet during sudden discharge from a pipe, Int. J. Hydrog. Energy 34 (2009) 5810–5816.

[7] S. Golovastov, D. Baklanov, V. Volodin, V. Golub, K. Ivanov, An experimental study of the diffusion-controlled self-ignition of hydrogen in a channel, Russ. J. Phys. Chem. B 3 (2009) 348–355.

[8] P. Oleszczak, P. Wolanski, Investigation of hydrogen ignition during outflow into atmosphere from high pressure system, in: 22nd Intl Colloquium on the Dynamics of Explosions and Reactive Systems, 2009.

[9] N. Rezaeyan, L. Bauwens, M. I. Radulescu, F. Fachini, The crucial role of the lewis number in jet ignition (2011).

[10] B. Maxwell, M. Radulescu, Ignition limits of rapidly expanding diffusion layers: Application to unsteady hydrogen jets, Combust. Flame 158 (2011) 1946–1959.

[11] A. Smygalina, A. Kiverin, Self-ignition of hydrogen jet due to interaction with obstacle in the obstructed space, Int. J. Hydrog. Energy 47 (2022) 35877–35885.

[12] P. Boivin, C. Jiménez, A. L. Sánchez, F. A. Williams, An explicit reduced mechanism for h2–air combustion, Proc. Combust. Inst. 33 (2011) 517–523.

[13] D. G. Goodwin, H. K. Moffat, R. L. Speth, Cantera: An object-oriented software toolkit for chemical kinetics, thermodynamics, and transport processes, `http://www.cantera.org` (2017).

[14] E. F. Toro, Riemann solvers and numerical methods for fluid dynamics: a practical introduction, Springer Science & Business Media, 2013.

[15] M. I. Radulescu, C. K. Law, The transient start of supersonic jets, J. Fluid Mech. 578 (2007) 331–369.

[16] K. Schmidmayer, F. Petitpas, S. Le Martelot, É. Daniel, Ecogen: An open-source tool for multiphase, compressible, multiphysics flows, Comput. Phys. Commun. 251 (2020) 107093.

[17] M. Le Boursicaud, S. Zhao, J.-L. Consalvi, P. Boivin, An improved passive scalar model for hydrogen hazardous ignition prediction, Combust. Flame 256 (2023) 112938.

[18] P. Boivin, A. Sánchez, F. Williams, Analytical prediction of syngas induction times, Combust. Flame 176 (2017) 489–499.

[19] P. Boivin, A. L. Sánchez, F. A. Williams, Explicit analytic prediction for hydrogen–oxygen ignition times at temperatures below crossover, Combust. Flame 159 (2012) 748–752.

[20] B. P. Xu, L. E. Hima, J. X. Wen, V. Tam, Numerical study of spontaneous ignition of pressurized hydrogen release into air, Int. J. Hydrog. Energy 34 (2009) 5954–5960.

[21] Y.-L. Liu, J.-Y. Zheng, P. Xu, Y.-Z. Zhao, H.-Y. Bie, H.-G. Chen, H. Dryver, Numerical simulation on the diffusion of hydrogen due to high pressured storage tanks failure, J. Loss Prev. Process Ind. 22 (2009) 265–270.

[22] A. L. Sánchez, E. Fernández-Tarrazo, P. Boivin, A. Liñán, F. A. Williams, Ignition time of hydrogen–air diffusion flames, C.R. Mec. 340 (2012) 882–893.

[23] T. Poinsot, D. Veynante, Theoretical and numerical combustion, RT Edwards, Inc., 2005.

[24] J. Li, Z. Zhao, A. Kazakov, F. L. Dryer, An updated comprehensive kinetic model of hydrogen combustion, Int. J. Chem. Kinet. 36 (2004) 566–575.

Appendix A. Simplification of the diffusion layer for 2 species

When using the scalar approach, no reaction nor heat released are considered, meaning that only the main species H_2, O_2 and N_2 can be present. Moreover, in our case the O_2 and N_2 are present together, due to the similarity of those two molecules, we can describe them as one equivalent air specie as done in [22] for example. Only one mass fraction is then required to describe the composition as Y_{O_2}=0.233Y_{air}=0.233(1-Y_{H_2}) or X_{O_2}=0.21X_{air}=0.21(1-X_{H_2}), leading to:

$$\frac{\partial Y_{H_2}}{\partial t} = \frac{\partial}{\partial m}\left(\rho^2 D_{H_2}\frac{W_{H_2}}{W}\frac{\partial X_{H_2}}{\partial m}\right), \tag{A.1}$$

$$\begin{aligned}\rho c_p \frac{\partial T}{\partial t} =& \frac{Dp}{Dt} + \rho\frac{\partial}{\partial m}\left(\rho\kappa\frac{\partial T}{\partial m}\right) + \\ & \frac{\rho^3}{W}\left(D_{H_2}W_{H_2}c_{p,H_2} - D_{\text{air}}W_{\text{air}}c_{p,\text{air}}\right)\frac{\partial X_{H_2}}{\partial m}\frac{\partial T}{\partial m}.\end{aligned} \tag{A.2}$$

As explained in section 2.1, D_{H_2} is the mixture average diffusion coefficient, meaning that it is the hydrogen diffusion with respect to the local mixture, and it is computed from the binary diffusion coefficient $D_{j,k}$ of the species considered, the general formula (also used in Cantera) is [23]:

$$D_k = \frac{1 - Y_k}{\sum_{j\neq k} X_j D_{j,k}}. \tag{A.3}$$

Applied for the hydrogen it gives:

$$D_{H_2} = \frac{1 - Y_{H_2}}{0.21X_{\text{air}}/D_{H_2,O_2} + 0.79X_{\text{air}}/D_{H_2,N_2}}, \tag{A.4}$$

it can be rewrite, using the equivalent binary diffusion coefficient of the hydrogen/air couple:

$$D_{H_2,\text{air}} = \frac{1}{0.21/D_{H_2,O_2} + 0.79/D_{H_2,N_2}}. \tag{A.5}$$

(A.4) and (A.1) become:

$$D_{H_2} = \frac{Y_{\text{air}}}{X_{\text{air}}/D_{H_2,\text{air}}} = \frac{W_{\text{air}}}{W}D_{H_2,\text{air}}, \tag{A.6}$$

$$\frac{\partial Y_{\mathrm{H_2}}}{\partial t} = \frac{\partial}{\partial m}\left(\rho^2 D_{\mathrm{H_2,air}} \frac{W_{\mathrm{H_2}} W_{\mathrm{air}}}{W^2} \frac{\partial X_{\mathrm{H_2}}}{\partial m}\right) = \frac{\partial}{\partial m}\left(\rho^2 D_{\mathrm{H_2,air}} \frac{\partial Y_{\mathrm{H_2}}}{\partial m}\right). \quad \text{(A.7)}$$

We fall back to the Fick law, a preferable option when only two species are considered, the equivalent diffusion velocity (needed in the temperature equation) gives:

$$Y_{\mathrm{H_2}} V_{\mathrm{H_2}} = -Y_{\mathrm{air}} V_{\mathrm{air}} = -\rho D_{\mathrm{H_2,air}} \frac{\partial Y_{\mathrm{H_2}}}{\partial m}, \quad \text{(A.8)}$$

therefore, the temperature equation now reads:

$$\rho c_p \frac{\partial T}{\partial t} = \frac{Dp}{Dt} + \rho \frac{\partial}{\partial m}\left(\rho \kappa \frac{\partial T}{\partial m}\right) + \rho^3 \left(c_{p,\mathrm{H_2}} - c_{p,\mathrm{air}}\right) D_{\mathrm{H_2,air}} \frac{\partial Y_{\mathrm{H_2}}}{\partial m} \frac{\partial T}{\partial m}. \quad \text{(A.9)}$$

Even if equations (A.7) and (A.9) have the simplest formulation, the one with the mixture average diffusion will be kept in section 4 to avoid confusion, as the two formulations are equivalent.

Appendix B. Impact of chemical kinetics description

To further validate the use of the 8-step skeletal mechanism, we compared the final ignition limits obtained with this mechanism and with the detailed mechanism used in the original study [10]. It is a 19-step detailed mechanism described in [24], it contains all of the reactions of the skeletal mechanism, however the reaction rates can be slightly different.

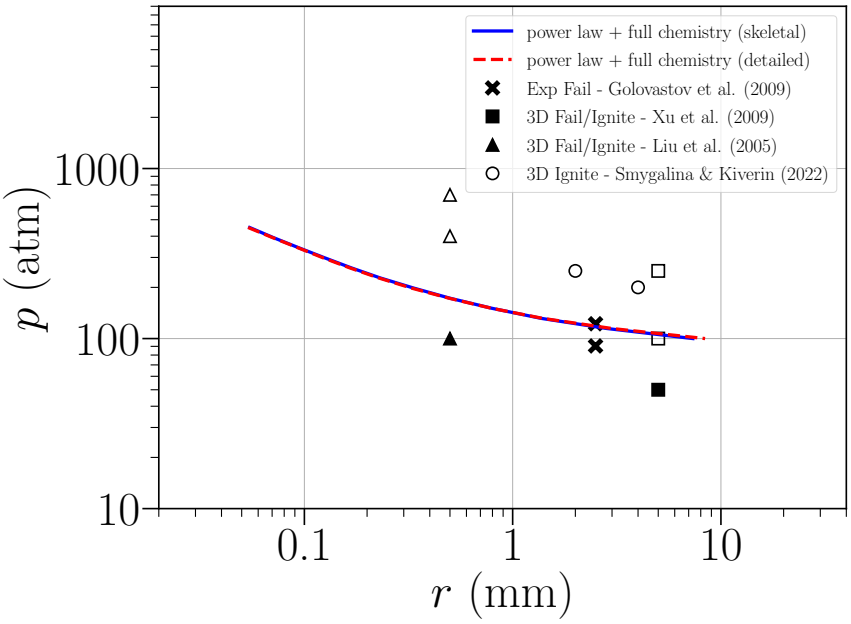

Figure B.15: Comparison of the ignition limits obtained with the skeletal and detailed mechanisms.

Figure B.15 displays no evident difference in the final ignition limit when using the different chemistry descriptions, motivating therefore the use of the skeletal approach for its simplicity.

Appendix C. Application to other geometries

To adapt our approach to the pipe configuration described in section 5.2, only the source term shape function needs to be changed, Eq. (22) is replaced by:

$$\mathcal{S}_{\text{pipe}}(x,t) = \begin{cases} 0, & \text{if } t < t_E \text{ or } x < 0 \\ \frac{\alpha}{r}\frac{13\chi^2+8\chi}{13\chi^3+4\chi+51}, & \text{otherwise} \end{cases}, \tag{C.1}$$

the resulting source term coefficient is compared to the one obtained from a 2D simulation in Fig. C.16. The pipe source term is always 0 for negative $\chi{=}x/r$ values, as it correspond to the domain inside the pipe, where the flow is purely one-dimensional.

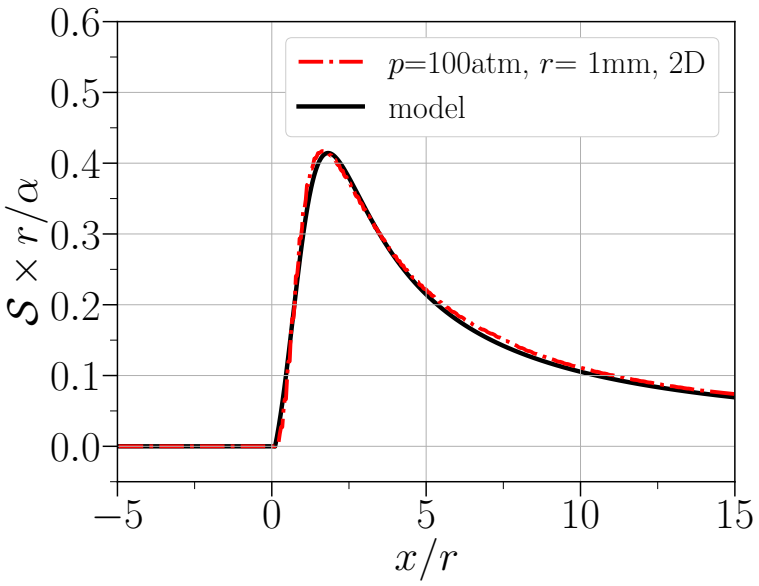

Figure C.16: Comparison of the dimensionless source term coefficients profiles $\mathcal{S}$ obtained as post-treatment of a 2D ECOGEN simulation and the model given by Eq. (C.1).

Figure C.17 shows the flow fields for the pipe configuration in the same conditions as those in Fig. 2. The pressure and temperature are lower than the tank configuration, which is to be expected since a pipe cannot sustain a leakage as strong as the one of a tank.

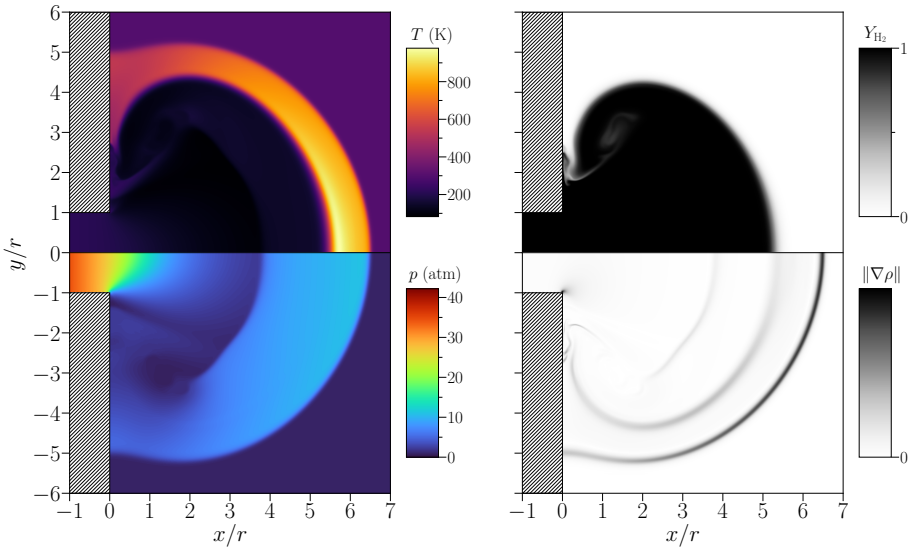

Figure C.17: Temperature (top left), pressure (bottom left), hydrogen mass fraction (top right) and density gradient (bottom right) fields obtained with ProLB [2] for a hydrogen tank pressure of p_{tank}=100 atm and a leakage radius of r=2 mm at a time t=10 µs.

Appendix D. Applicability to other conditions

To study the applicability of the proposed pseudo-1D model to other gases, ECOGEN simulations of high-pressure helium, air, methane, propane, and carbon dioxide leakage into ambient air were performed. The results suggest that the pressurized gas molecular weight and heat capacity ratio (γ_{He}=1.666, γ_{CH_4}=1.313, $\gamma_{\text{C}_3\text{H}_8}$=1.13, γ_{CO_2}=1.3) have almost no impact, as the simulations give the same self-similar source term profiles. Figure D.18 shows the dimensionless source term $\mathcal{S} \times r/\alpha$ as a function of the dimensionless coordinate χ=x/r for the different gases, highlighting the self-similarity of the profiles for all the gases tested. In addition, other simulations of the hydrogen leakage case were performed with different hydrogen and air initial temperatures, and no impact of these initial conditions was found. Figure D.19 shows the dimensionless source term as a function of the dimensionless coordinate for the different initial temperatures, highlighting the self-similarity of the profiles for all the conditions tested. Therefore, the source term models proposed in Eqs. (22) and (C.1) can be directly used to recover the flow of high-pressure leakage of these gases for a large range of initial temperatures between the tank and the air.

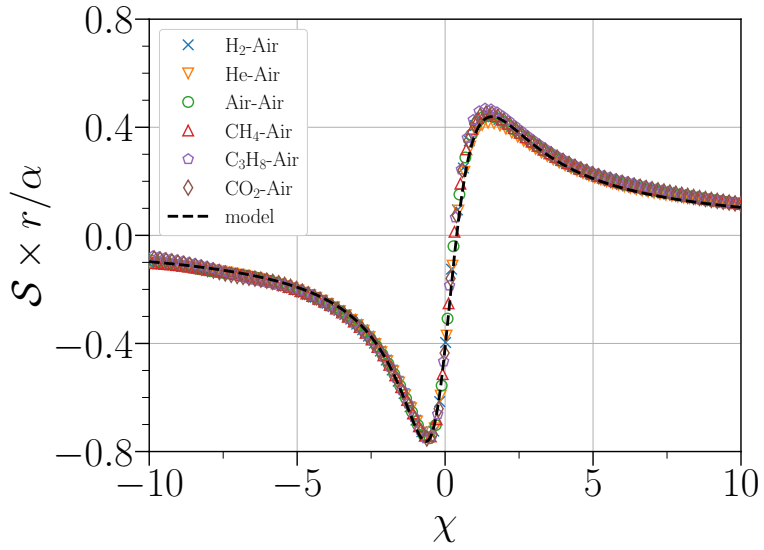

Figure D.18: Comparison of the source term coefficient $\mathcal{S}$ profiles for high-pressure leakage of different gases from a tank into ambient air, as obtained by post-treatment of two-dimensional ECOGEN simulations. The tank source term model, given by Eq. (22), is also represented (black dashed curve).

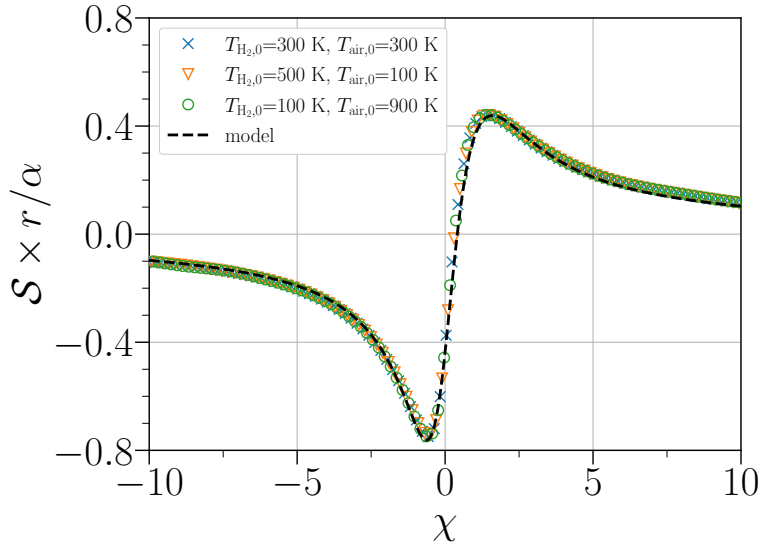

Figure D.19: Comparison of the source term coefficient $\mathcal{S}$ profiles for a high-pressure hydrogen tank leakage into atmospheric pressure air for different hydrogen and air initial temperatures, as obtained by post-treatment of two-dimensional ECOGEN simulations. The tank source term model, given by Eq. (22), is also represented (black dashed curve).